Spatio-Temporal Model Reduction of Inverter-Based Islanded Microgrids

Ling Luo and Sairaj V. Dhople, *Member, IEEE*

***Abstract*—Computationally efficient and scalable models that describe droop-controlled inverter dynamics are key to modeling, analysis, and control in islanded microgrids. Typical models developed from first principles in this domain describe detailed dynamics of the power electronics inverters as well as the network interactions. Consequently, these models are very involved; they offer limited analytical insights and are computationally expensive when applied to investigate the dynamics of large microgrids with many inverters. This calls for the development of reduced-order models that capture the relevant dynamics of higher-order models with a lower dimensional state space while not compromising modeling fidelity. To this end, this paper proposes model reduction methods based on singular perturbation and Kron reduction to reduce large-signal dynamic models of inverter-based islanded microgrids in temporal and spatial aspects, respectively. The reduced-order models are tested in a modified IEEE 37-bus system and verified to accurately describe the original dynamics with lower computational burden. In addition, we demonstrate that Kron reduction isolates the mutual inverter interactions and the equivalent loads that the inverters have to support in the microgrid—this aspect is leveraged in the systematic selection of droop coefficients to minimize power losses and voltage deviations.**

***Index Terms*—Droop control, Islanded microgrid, Kron reduction, Model reduction, Singular perturbation.**

I. INTRODUCTION

INVERTER-interfaced islanded microgrids serve the primary objective of meeting critical loads while maintaining frequency and voltage within prescribed performance limits. Inspired by the operation and control of synchronous machines in bulk power systems, droop control is an effective primary-level control strategy that has widely been applied in this domain [1]. The premise of droop control is to trade off voltage and frequency based on the active and reactive power injected by the power electronic inverters in the microgrid. Control synthesis, performance evaluation, stability analysis, and reliability estimation of inverter-interfaced microgrids require scalable and computationally efficient models that accurately capture the dynamics of droop-controlled inverters and describe all interactions between the constituent sources, loads, and power electronic inverters. However, typical models for droop-controlled inverters are very detailed, and include myriad states from internal control loops and filters [2]–[6]. Conceivably, control design, numerical simulations, and stability assessment with such models in islanded microgrids comprising tens of or even hundreds of inverters is computationally expensive and offers limited analytical insights. These aspects call for the development of model-reduction methods to isolate relevant spatio-temporal dynamics and mutual interactions of interest. While model reduction methods are well established for synchronous generators in bulk power systems, a systematic model-reduction procedure for droop-controlled islanded inverters has thus far been lacking. This paper proposes model reduction methods based on singular perturbation and Kron reduction to reduce large-signal dynamic models of inverter-based islanded microgrids in temporal and spatial aspects, respectively.

As mentioned above, related to this work are model reduction techniques for dynamic models in bulk power systems. Examples include Krylov subspace methods [7], Gramian-based methods [8], aggregate slow coherency [9], and singular perturbation methods [10]–[12]. Moment matching model reduction by projection on Krylov subspaces is proposed in [7] to reduce the power system dynamical model order. Gramian-based methods proposed in [8] reduce model order by computing approximations to the controllability and observability gramians of large sparse power system models. Aggregate slow coherency methods used in bulk power system analysis, simulations and islanding strategy studies [13], [14] are implemented with steps of linearization, calculation of eigenvalues and eigenvectors, and systematic division into coherent groups. Singular perturbation methods provide a systematic approach to multiple time scales modeling in dynamical systems with state variables that evolve at different speeds [15]–[17]. In singular perturbation methods, reduced-order models are obtained by identifying fast variables and subsequently neglecting their dynamics in a systematic fashion (this amounts to assuming they reach steady state much faster than the slow variables in the system) [10], [12], [16], [18]. Related to our approach, singular perturbation methods were applied in [19] to obtain reduced-order models neglecting load dynamics in parallel-connected droop-controlled inverters. Since the proposed approach applies to circuits that lie at the intersection of power electronics and power systems, another body of related work pertains to model reduction methods that have been applied in the domain of power electronics circuits, see, e.g., [20]–[23] and the references therein.

Compared to Krylov-subspace, Gramian-based, and slow-coherency methods which require linearization and calculation of eigenvalues, singular perturbation methods are much more intuitive to construct in dynamical models composed of differential equations with multiple time scales. Given these advantages, reduced-order models for droop-controlled inverters are obtained by applying singular-perturbation methods.

This work was supported by the Institute of Renewable Energy and the Environment (IREE) grant no. RL-0011-13, University of Minnesota.

The authors are with the Department of Electrical and Computer Engineering at the University of Minnesota, Minneapolis, MN, 55455 (email: luoxx297,sdhople@UMN.EDU).

In addition, Kron reduction is utilized to reduce the network in the spatial aspect by eliminating the algebraic power-flow equations corresponding to the loads and other nodes in the network that are not connected to the inverters. Originally proposed in 1953 [24], Kron reduction is a standard model reduction tool employed in power networks for applications such as transient stability assessment [25], [26]. Here, the tool eliminates exogenous non-inverter nodes and isolates the mutual inverter interactions and the equivalent loads that the inverters have to satisfy.

We demonstrate the model reduction methodology with the the large-signal dynamic model of droop-controlled inverters described in [2] chosen as a benchmark. The inverter control system is composed of a power controller (within which the droop control laws are embedded), as well as additional loops for voltage and current control. The model includes differential equations with multiple time scales which motivates the application of singular-perturbation methods for model reduction. The model in [2] is chosen as a benchmark to ensure the results are widely accessible to researchers and practising engineers; in particular, our choice is motivated by the fact that similar models have been utilized in [6], [27]–[33]. The approach to model reduction is presented with a broad level of generality so it can be adopted by researchers and practicing engineers in other settings. A particularly interesting result of the model-reduction procedure is that the ubiquitous first-order droop law that is commonly employed in modeling, analysis, and control (see, e.g., [34]) is recovered from the full nonlinear dynamical system after successive applications of singular perturbation.

The remainder of this paper is organized as follows. Section II introduces the large-signal dynamic model of an inverter-based islanded microgrid, including the model of a single inverter, the coordinate transformations involved in incorporating multiple inverters, and the electrical network. Section III presents: i) the temporal model reduction approach based on singular perturbation methods, and ii) the spatial model reduction approach based on Kron reduction. Section IV includes numerical simulation studies to validate the spatio-temporal reduced models in a modified IEEE 37-bus network. In addition, a strategy for the systematic selection of droop coefficients to minimize power losses and voltage deviations is also presented. We anticipate this approach being complementary to recent work that has addressed the optimal design of droop coefficients and laws from the perspectives of energy-storage management, power sharing, and economic optimization [35]–[37]. Concluding remarks and directions for future work are presented in Section V.

II. System Model

In this section, the large-signal nonlinear differential algebraic system model of inverter-based islanded microgrids is introduced. We first present the model of a single inverter, and then describe the microgrid network model.

A. Inverter Model

Consider an islanded microgrid comprising N droop-controlled inverters, and suppose all loads in the microgrid are modeled either as constant impedances or constant current sources. Figure 1 shows a block diagram of the controller employed in each inverter. In addition to the power controller (within which the droop laws are embedded) there are additional inner control loops to regulate the inverter output current and terminal voltage. Let ω denote the electrical frequency of the inverter, and let ω_{com} denote an adopted common electrical frequency. (For modeling purposes, this is typically chosen to be the electrical frequency of some inverter in the system. In this work, we assume that inverter $i = 1$ sets the common frequency.) Then, the evolution of the power angle of the inverter, δ, (defined with respect to the power angle of the reference inverter) is governed by

$$\frac{d\delta}{dt} = \omega - \omega_{\mathrm{com}}, \tag{1}$$

Consequently, we can transform the terminal voltage and output current for each inverter from abc to dq coordinates, using the terminal voltage angle $\delta + \omega_{\mathrm{com}} t$ as the reference frame angle to obtain $v_{\mathrm{o}} := v_{\mathrm{od}} + \mathrm{j} v_{\mathrm{oq}}$ and $i_{\mathrm{o}} := i_{\mathrm{od}} + \mathrm{j} i_{\mathrm{oq}}$. The dynamical equation that captures the operation of the power controller is given by:

$$\frac{1}{\omega_{\mathrm{c}}} \frac{dS}{dt} = -S + v_{\mathrm{o}} i_{\mathrm{o}}^{*}, \tag{2}$$

where ω_{c} is the cut-off frequency, and $S = P + \mathrm{j}Q$ is the apparent (low-pass filtered) power delivered by the inverter.[1] The outputs of the power controller are the voltage reference and the inverter frequency governed by the voltage-reactive power droop law, and the frequency-active power droop law [2], [6], [27]–[33], [37], [38]:

$$v_{\mathrm{o}}^{\mathrm{ref}} = v_{\mathrm{nom}} - n_{\mathrm{Q}} Q = v_{\mathrm{nom}} - n_{\mathrm{Q}} \frac{S - S^{*}}{2}, \tag{3}$$

$$\omega = \omega_{\mathrm{nom}} - m_{\mathrm{P}} P = \omega_{\mathrm{nom}} - m_{\mathrm{P}} \frac{S + S^{*}}{2}, \tag{4}$$

where v_{nom} and ω_{nom} are the nominal system voltage and frequency, respectively. The droop coefficients, n_{Q} and m_{P}, are the slopes of the voltage-reactive power and frequency-active power curves, respectively, and they are set as:

$$m_{\mathrm{P}} = \frac{\Delta\omega}{P_{\mathrm{max}}}, \quad n_{\mathrm{Q}} = \frac{\Delta V}{Q_{\mathrm{max}}}, \tag{5}$$

[1] *Notation:* $(\cdot)^{\mathrm{T}}$ denotes transposition; $(\cdot)^{*}$ denotes the complex conjugate; $\mathrm{Re}\{\cdot\}$ and $\mathrm{Im}\{\cdot\}$ denote the real and imaginary parts of a complex number, respectively; and $\mathrm{j} := \sqrt{-1}$ is the imaginary unit. The (p, q) entry of the matrix A is denoted by $[A]_{pq}$.

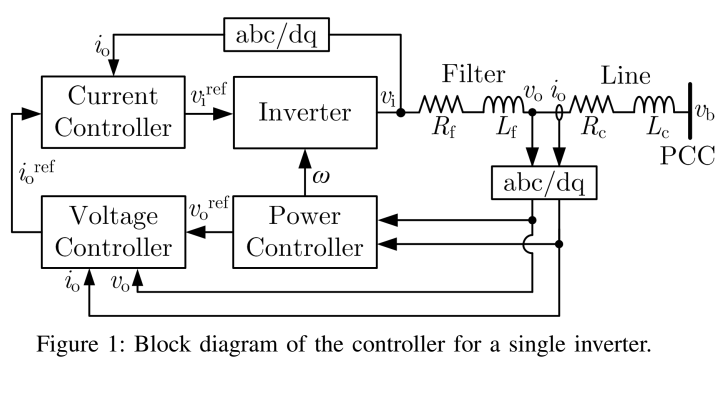

Figure 1: Block diagram of the controller for a single inverter.

where $P_{\max}$ ($Q_{\max}$) is the maximum active power (reactive power) that the inverter is expected to deliver to support frequency (terminal voltage), and $\Delta\omega$ (ΔV) is the permissible frequency (voltage) deviation. For the inverter selected to be the common reference inverter, the frequency is given by

$$\omega_{\mathrm{com}} = \omega_{\mathrm{nom}} - m_{\mathrm{P}} P = \omega_{\mathrm{nom}} - m_{\mathrm{P}} \frac{S + S^*}{2}. \tag{6}$$

The voltage- and current-controller state variables are denoted by $\phi = \phi_{\mathrm{d}} + \mathrm{j}\phi_{\mathrm{q}}$ and $\gamma = \gamma_{\mathrm{d}} + \mathrm{j}\gamma_{\mathrm{q}}$, respectively. Following [2], [3], [6], [39], a conventional PI controller is utilized to regulate the terminal voltage and output currents to their reference values, denoted by $v_{\mathrm{o}}^{\mathrm{ref}}$ and $i_{\mathrm{o}}^{\mathrm{ref}}$, respectively. The voltage and current controllers generate the references

$$i_{\mathrm{o}}^{\mathrm{ref}} = F i_{\mathrm{o}} + K_{\mathrm{p}}^{\phi} \frac{d\phi}{dt} + K_{\mathrm{i}}^{\phi} \phi, \tag{7}$$

$$v_{\mathrm{i}}^{\mathrm{ref}} = \mathrm{j}\omega_{\mathrm{nom}} L_{\mathrm{f}} i_{\mathrm{o}} + K_{\mathrm{p}}^{\gamma} \frac{d\gamma}{dt} + K_{\mathrm{i}}^{\gamma} \gamma, \tag{8}$$

where K_{p}^{ϕ} (K_{p}^{γ}) and $K_{\mathrm{i}}^{\phi}(K_{\mathrm{i}}^{\gamma})$ are the parameters for the current (voltage) PI control blocks, and F is the static gain of the current feedforward control block. The controller dynamics are governed by

$$\frac{d\phi}{dt} = v_{\mathrm{o}}^{\mathrm{ref}} - v_{\mathrm{o}}, \quad \frac{d\gamma}{dt} = i_{\mathrm{o}}^{\mathrm{ref}} - i_{\mathrm{o}}. \tag{9}$$

For control purposes, the quadrature component of the reference terminal voltage $v_{\mathrm{oq}}^{\mathrm{ref}}$ is set to zero, and $v_{\mathrm{o}}^{\mathrm{ref}} = v_{\mathrm{od}}$ as shown in Fig. 2. Finally, the dynamics of the output current are captured by

$$\frac{L_{\mathrm{c}}}{R_{\mathrm{c}}} \frac{di_{\mathrm{o}}}{dt} = -\left(1 + \mathrm{j}\omega \frac{L_{\mathrm{c}}}{R_{\mathrm{c}}}\right) i_{\mathrm{o}} + \frac{v_{\mathrm{o}} - v_{\mathrm{b}}}{R_{\mathrm{c}}}, \tag{10}$$

where $v_{\mathrm{b}} := v_{\mathrm{bd}} + \mathrm{j}v_{\mathrm{bq}}$ is the bus voltage at the point of common coupling (PCC). Equations (1), (2), (9), and (10) describe the large-signal ninth-order dynamical model of a single inverter in the dq reference frame. Note that the following dynamic states are included in this model: δ, P, Q, ϕ_{d}, ϕ_{q}, γ_{d} γ_{q}, i_{od}, and i_{oq}.

In practical microgrids, a common reference frame has to be adopted for all the inverters since there are multiple inverters in the system. We denote the common reference frame as the DQ reference frame, and suppose it is specified by the $i = 1$ inverter. When inverters are integrated to the microgrid through the PCC, the PCC voltage and output current should be transformed to the common reference frame DQ-axis by

$$v_{\mathrm{o}}^{\mathrm{DQ}} = T v_{\mathrm{o}}, \quad i_{\mathrm{o}}^{\mathrm{DQ}} = T i_{\mathrm{o}}, \tag{11}$$

where the dq to DQ-axis transformation matrix, T, is:

$$T = \begin{bmatrix} 1 & 0 & \cdots & 0 \\ 0 & e^{\mathrm{j}\delta_2} & \cdots & 0 \\ \vdots & \vdots & \ddots & \vdots \\ 0 & 0 & \cdots & e^{\mathrm{j}\delta_N} \end{bmatrix}. \tag{12}$$

Notice that the $(1,1)$ entry of T, $[T]_{11} = 1$, since $\delta_1(t) = 0$ by definition in (1).

B. Network Model

Given the high switching frequency of the inverters, the dynamics of the transmission lines and loads are neglected and network interactions are described by algebraic relations based on Ohm's and Kirchoff's laws.

Suppose, that in addition to the N inverter buses, the microgrid includes M buses, that may be connected to loads. The microgrid buses are collected in the set $\mathcal{A} := \{1, \ldots, N+M\}$, and distribution lines are represented by the set $\mathcal{E} := \{(p,q)\} \subset \mathcal{A} \times \mathcal{A}$. The series admittance of the line (p, q) is denoted by $y_{pq} = (R_{pq} + \mathrm{j}\omega_{\mathrm{com}} L_{pq})^{-1}$, where R_{pq}, L_{pq}, and ω_{com} denote the line resistance, inductance, and the common angular frequency. Let $Y \in \mathbb{C}^{N+M \times N+M}$ denote the complex admittance matrix of the network, v, i denote the vectors of bus voltage and nodal current injections (expressed in DQ coordinates). Expressing Kirchoff's circuit laws in matrix-vector form, we can write

$$i = Yv, \tag{13}$$

where the entries of Y are defined as

$$[Y]_{pq} := \begin{cases} \sum_{j \in \mathcal{N}_p} y_{pj}, & \text{if } p = q \\ -y_{pq}, & \text{if } (p,q) \in \mathcal{E} \\ 0, & \text{otherwise} \end{cases}$$

and $\mathcal{N}_p := \{j \in \mathcal{A} : (p,j) \in \mathcal{E}\}$ denotes the set of buses connected to the p^{th} bus through a distribution line.

III. Spatio-Temporal Model Reduction

In Section II, we described the complete large-signal dynamic model for droop-controlled inverters that includes states from multiple internal control loops and filters [2], [3], [6]. In this section, we describe how Kron reduction allows us to simplify the network equations, and how singular perturbation methods allow us to derive reduced models of different orders for individual inverters.

A. Kron Reduction

Kron reduction is a standard tool employed in modeling, analysis, and control of power systems (see [26] and references therein for a detailed overview). In this work, Kron reduction is utilized to eliminate internal, non-inverter buses, and isolate the mutual inverter interactions.

Recall from Section II, the interactions of the inverters and loads within the electrical network are described by (13). To

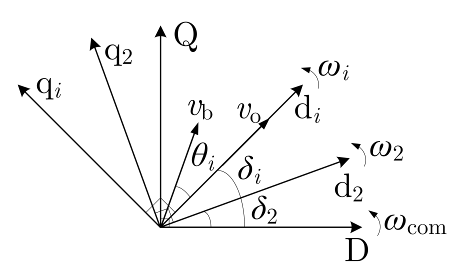

Figure 2: Angle reference frames for multiple inverters.

eliminate the non-inverter buses, first we divide the buses into two groups, and let $v_{\mathcal{N}} \in \mathbb{C}^{N\times 1}$ ($v_{\mathcal{M}} \in \mathbb{C}^{M\times 1}$) denote the vector of voltages of the nodes connected (not connected, respectively) to inverters. Similarly, let $i_{\mathcal{N}} \in \mathbb{C}^{N\times 1}$ ($i_{\mathcal{M}} \in \mathbb{C}^{M\times 1}$) denote the vector of current injections at the nodes connected (not connected, respectively) to the inverters. Note that non-zero elements in the vector $i_{\mathcal{M}}$ denote constant-current loads. Then (13) can be expressed as

$$\begin{bmatrix} i_{\mathcal{N}} \\ i_{\mathcal{M}} \end{bmatrix} = \begin{bmatrix} Y_{\mathcal{N}\mathcal{N}} & Y_{\mathcal{N}\mathcal{M}} \\ Y_{\mathcal{N}\mathcal{M}}^{\mathrm{T}} & Y_{\mathcal{M}\mathcal{M}} \end{bmatrix} \begin{bmatrix} v_{\mathcal{N}} \\ v_{\mathcal{M}} \end{bmatrix}. \tag{14}$$

Eliminating $v_{\mathcal{M}}$ from the equation above allows us to write:

$$i_{\mathcal{N}} = Y_{\mathrm{eq}} v_{\mathcal{N}} + Y_{\mathcal{N}\mathcal{M}} Y_{\mathcal{M}\mathcal{M}}^{-1} i_{\mathcal{M}}, \tag{15}$$

$$Y_{\mathrm{eq}} = Y_{\mathcal{N}\mathcal{N}} - Y_{\mathcal{N}\mathcal{M}} Y_{\mathcal{M}\mathcal{M}}^{-1} Y_{\mathcal{N}\mathcal{M}}^{\mathrm{T}}, \tag{16}$$

where Y_{eq} is referred subsequently as the *Kron reduced admittance matrix*.

From (16), it is evident that we assume the matrix $Y_{\mathcal{M}\mathcal{M}}$ is nonsingular. This implies that the non-inverter node voltages have a unique solution, given by $v_{\mathcal{M}} = -Y_{\mathcal{M}\mathcal{M}}^{-1} Y_{\mathcal{N}\mathcal{M}}^{\mathrm{T}} v_{\mathcal{N}}$. Indeed, it is important to qualify the class of networks for which $Y_{\mathcal{M}\mathcal{M}}$ is nonsingular. For RLC networks with shunt elements, it is possible to obtain a singular $Y_{\mathcal{M}\mathcal{M}}$, such that the interior voltages $v_{\mathcal{M}}$ are not uniquely determined (this can happen, e.g., when capacitive lines exactly cancel out inductive loads). However, for RLC networks without shunt elements, the matrix $Y_{\mathcal{M}\mathcal{M}}$ is always nonsingular because $Y_{\mathcal{A}}$ is irreducibly block diagonally dominant [40], [41]. In this paper, we assume that $Y_{\mathcal{M}\mathcal{M}}$ is always nonsingular.

Basically, (16) indicates that the inverter current injections and terminal voltages are coupled through Y_{eq}; furthermore, constant-current loads in the network are mapped to individual inverters through the matrix $Y_{\mathcal{N}\mathcal{M}} Y_{\mathcal{M}\mathcal{M}}^{-1}$. Note that the diagonal entries of Y_{eq} capture the equivalent local loads that each inverter has to support, and off-diagonal entries indicate equivalent impedances that couple inverters.

The overall dynamic model of the inverters in the microgrid is composed of two parts: i) the differential-algebraic equations for the inverters, and ii) the algebraic equations of the network. For simplicity of discussion, here we assume there are only impedance loads in the network (i.e., $i_{\mathcal{M}} = 0$ in (16)). For the purpose of simulation, first, we solve for the vector of bus voltages as: $v_{\mathcal{N}} = Y_{\mathrm{eq}}^{-1} i_{\mathcal{N}}$, with $i_{\mathcal{N}} = T i_{\mathrm{o}}$ and $v_{\mathcal{N}} = T v_{\mathrm{b}}$. Then, the PCC bus voltage vector is transformed from DQ-axis to the dq-axis as input of the inverter differential equations by setting $u = v_{\mathrm{b}} = T^{-1} Y_{\mathrm{eq}}^{-1} T i_{\mathrm{o}}$.

Note that applying Kron reduction restricts our attention to loads that are combinations of impedances and current sources/sinks. Constant power loads have to be approximated as equivalent impedances as is done commonly in transient stability assessment studies for synchronous generators in bulk power systems [42].

B. Singular Perturbation Methods

For dynamical systems which exhibit different dynamic response speeds, singular perturbation methods can be applied to reduce the model order by neglecting the fast dynamic state variables. The premise is to assume that the fast dynamic variables instantaneously reach a quasi-steady-state solution which can be obtained by the solution of algebraic equations that result from relevant originating dynamical equations [10], [12], [16], [18], [43]. To formalize the presentation, the microgrid dynamic model with multiple time scales is expressed in the following standard singular perturbation form [10], [11], [44]:

$$\frac{dx}{dt} = f(x, z, u, t, \varepsilon), \tag{17}$$

$$\varepsilon \frac{dz}{dt} = g(x, z, u, t, \varepsilon), \tag{18}$$

where $x \in \mathbb{C}^{n\times 1}$, is the vector that collects the slow dynamic variables, $z \in \mathbb{C}^{m\times 1}$, is the vector that collects the fast dynamic variables, u is the vector of inputs, and $\varepsilon = \mathrm{diag}\{\varepsilon_1, \varepsilon_2, \cdots, \varepsilon_m\}$ denotes a diagonal matrix with non-zero entries comprised of small model parameters.

From [11], [44], if the Jacobian of $g(\cdot)$, given by

$$\left. \frac{\partial g(x, z, u, t, \varepsilon)}{\partial z} \right|_{\varepsilon=0}, \tag{19}$$

is nonsingular with eigenvalues that have negative real parts, then we can reduce the $n+m$ order system in (17)-(18) to an n-order system. To this end, following [11, Theorem 11.1], we set $\varepsilon = 0$; obtain the quasi-steady-state (QSS) solution

$$z = h(x, u, t), \tag{20}$$

and substitute $h(x, u, t)$ in (17), to get the reduced-order model

$$\frac{dx}{dt} = f(x, h(x, u, t), u, t, 0) =: \widetilde{f}(x, u, t). \tag{21}$$

In the next section, we apply the general method described above to successively reduce the original large-signal inverter models to obtain reduced models of varying orders.

C. Reduced-Order Microgrid Models

First, we describe how the original ninth-order model described in Section II (with dynamic states $x = [\delta,\ P,\ Q,\ \phi_{\mathrm{d}},\ \phi_{\mathrm{q}},\ \gamma_{\mathrm{d}},\ \gamma_{\mathrm{q}},\ i_{\mathrm{od}},\ i_{\mathrm{oq}}]^{\mathrm{T}}$) can be reduced to a fifth-order model (with dynamic states $x = [\delta,\ P,\ Q,\ i_{\mathrm{od}},\ i_{\mathrm{oq}}]^{\mathrm{T}}$) by eliminating the dynamical equations for the voltage and current controllers. For the purpose of analysis, we will find it useful to write the current- and voltage-controller dynamical equations in (7) and (8) in the following form

$$\frac{K_{\mathrm{p}}^{\phi}}{K_{\mathrm{i}}^{\phi}} \frac{d\phi}{dt} = -\phi + \frac{i_{\mathrm{o}}^{\mathrm{ref}} - F i_{\mathrm{o}}}{K_{\mathrm{i}}^{\phi}}, \tag{22}$$

$$\frac{K_{\mathrm{p}}^{\gamma}}{K_{\mathrm{i}}^{\gamma}} \frac{d\gamma}{dt} = -\gamma + \frac{v_{\mathrm{i}}^{\mathrm{ref}} - \mathrm{j}\omega_{\mathrm{nom}} L_{\mathrm{f}} i_{\mathrm{o}}}{K_{\mathrm{i}}^{\gamma}}. \tag{23}$$

Then, let $\varepsilon = \mathrm{diag}\{\varepsilon_1, \varepsilon_2\} = \mathrm{diag}\left\{\frac{K_{\mathrm{p}}^{\phi}}{K_{\mathrm{i}}^{\phi}}, \frac{K_{\mathrm{p}}^{\gamma}}{K_{\mathrm{i}}^{\gamma}}\right\}$ denote the diagonal matrix with non-zero entries comprised of the small-perturbation parameters. With this choice, the ninth-order model described by (1), (2), (10), (22) and (23) can be expressed in the standard singular perturbation form in (17)-(18). In this particular case, $x = [\delta,\ S,\ i_{\mathrm{o}}]^{\mathrm{T}} \in \mathbb{C}^{3\times 1}$ is the

Table I: Successive Temporal Model Reduction with Singular Perturbation

	Fifth-order model	Third-order model	Single-order model
Slow variables, x	$[\delta,\ S,\ i_\mathrm{o}]^\mathrm{T}$	$[\delta,\ S]^\mathrm{T}$	δ
Fast variables, z	$[\phi,\gamma]^\mathrm{T}$	i_o	S
Small parameter, ε	$\mathrm{diag}\left\{\varepsilon_1,\varepsilon_2\right\}=\mathrm{diag}\left\{\frac{K_\mathrm{p}^\phi}{K_\mathrm{i}^\phi},\frac{K_\mathrm{p}^\gamma}{K_\mathrm{i}^\gamma}\right\}$	$\varepsilon_3=\frac{L_\mathrm{c}}{R_\mathrm{c}}$	$\varepsilon_4=\frac{1}{\omega_\mathrm{c}}$
Vector field, $f(\cdot)$	$\begin{bmatrix}\omega_\mathrm{nom}-m_\mathrm{P}\frac{S+S^*}{2}-\omega_\mathrm{com}\\ -\omega_\mathrm{c}S+\omega_\mathrm{c}v_\mathrm{o}i_\mathrm{o}^*\\ -\left(\frac{R_\mathrm{c}}{L_\mathrm{c}}+\mathrm{j}\omega\right)i_\mathrm{o}+\frac{v_\mathrm{o}-v_\mathrm{b}}{L_\mathrm{c}}\end{bmatrix}$	$\begin{bmatrix}\omega_\mathrm{nom}-m_\mathrm{P}\frac{S+S^*}{2}-\omega_\mathrm{com}\\ -\omega_\mathrm{c}S+\omega_\mathrm{c}v_\mathrm{o}^\mathrm{ref}i_\mathrm{o}^*\end{bmatrix}$	$\omega_\mathrm{nom}-m_\mathrm{P}\frac{S+S^*}{2}-\omega_\mathrm{com}$
Vector field, $g(\cdot)$	$\begin{bmatrix}-\phi+\frac{i_\mathrm{o}^\mathrm{ref}-Fi_\mathrm{o}}{K_\mathrm{i}^\phi}\\ -\gamma+\frac{v_\mathrm{i}^\mathrm{ref}-\mathrm{j}\omega_\mathrm{nom}L_\mathrm{f}i_\mathrm{o}}{K_\mathrm{i}^\gamma}\end{bmatrix}$	$-\left(1+\mathrm{j}\omega\varepsilon_3\right)i_\mathrm{o}+\frac{v_\mathrm{o}^\mathrm{ref}-u}{R_\mathrm{c}}$	$-S+v_\mathrm{o}^\mathrm{ref}i_\mathrm{o}^*$
QSS solution of z	$[\phi,\gamma]^\mathrm{T}=\left[\frac{(1-F)i_\mathrm{o}}{K_\mathrm{i}^\phi},\ \frac{v_\mathrm{i}^\mathrm{ref}-\mathrm{j}\omega_\mathrm{nom}L_\mathrm{f}i_\mathrm{o}}{K_\mathrm{i}^\gamma}\right]^\mathrm{T}$	$i_\mathrm{o}=\frac{v_\mathrm{o}^\mathrm{ref}-u}{R_\mathrm{c}}$	$S=v_\mathrm{o}^\mathrm{ref}i_\mathrm{o}^*=v_\mathrm{o}^\mathrm{ref}\left(\frac{v_\mathrm{o}^\mathrm{ref}-u}{R_\mathrm{c}}\right)^*$
Reduced-order model, $\widetilde{f}(\cdot)$	$\begin{bmatrix}\omega_\mathrm{nom}-m_\mathrm{P}\frac{S+S^*}{2}-\omega_\mathrm{com}\\ -\omega_\mathrm{c}S+\omega_\mathrm{c}v_\mathrm{o}^\mathrm{ref}i_\mathrm{o}^*\\ -\left(\frac{R_\mathrm{c}}{L_\mathrm{c}}+\mathrm{j}\omega\right)i_\mathrm{o}+\frac{v_\mathrm{o}^\mathrm{ref}-u}{L_\mathrm{c}}\end{bmatrix}$	$\begin{bmatrix}\omega_\mathrm{nom}-m_\mathrm{P}\frac{S+S^*}{2}-\omega_\mathrm{com}\\ -\omega_\mathrm{c}S+\omega_\mathrm{c}v_\mathrm{o}^\mathrm{ref}\left(\frac{v_\mathrm{o}^\mathrm{ref}-u}{R_\mathrm{c}}\right)^*\end{bmatrix}$	$\omega_\mathrm{nom}-m_\mathrm{P}v_\mathrm{o}^\mathrm{ref}\mathrm{Re}(i_\mathrm{o})-\omega_\mathrm{com}$

vector that collects the slow dynamic variables, $z=[\phi,\gamma]^\mathrm{T}\in\mathbb{C}^{2\times1}$ is the vector that collects the fast dynamic variables, and $u=v_\mathrm{b}$, i.e., the PCC bus voltage is adopted as the input. With reference to the notation in (17)-(18), the vector fields $f(\cdot)$ and $g(\cdot)$ are given by

$$f=\begin{bmatrix}\omega_\mathrm{nom}-m_\mathrm{P}\frac{S+S^*}{2}-\omega_\mathrm{com}\\ -\omega_\mathrm{c}S+\omega_\mathrm{c}v_\mathrm{o}i_\mathrm{o}^*\\ -\left(\frac{R_\mathrm{c}}{L_\mathrm{c}}+\mathrm{j}\omega\right)i_\mathrm{o}+\frac{v_\mathrm{o}-v_\mathrm{b}}{L_\mathrm{c}}\end{bmatrix}, \tag{24}$$

$$g=\begin{bmatrix}-\phi+\frac{i_\mathrm{o}^\mathrm{ref}-Fi_\mathrm{o}}{K_\mathrm{i}^\phi}\\ -\gamma+\frac{v_\mathrm{i}^\mathrm{ref}-\mathrm{j}\omega_\mathrm{nom}L_\mathrm{f}i_\mathrm{o}}{K_\mathrm{i}^\gamma}\end{bmatrix}. \tag{25}$$

The Jacobian of $g(\cdot)$, $\frac{\partial g}{\partial z}|_{\varepsilon=0}=\mathrm{diag}\{-1,-1\}$, which is nonsingular and has eigenvalues with negative real parts. Setting $\varepsilon=0$, the QSS solution for z is given by

$$z=[\phi,\gamma]^\mathrm{T}=\left[\frac{i_\mathrm{o}^\mathrm{ref}-Fi_\mathrm{o}}{K_\mathrm{i}^\phi},\ \frac{v_\mathrm{i}^\mathrm{ref}-\mathrm{j}\omega_\mathrm{nom}L_\mathrm{f}i_\mathrm{o}}{K_\mathrm{i}^\gamma}\right]^\mathrm{T}. \tag{26}$$

Additionally, note that when (26) is substituted in (7)-(8), we get $d\phi/dt=0$ and $d\gamma/dt=0$, which from (9) implies that $v_\mathrm{o}=v_\mathrm{o}^\mathrm{ref}$ and $i_\mathrm{o}=i_\mathrm{o}^\mathrm{ref}$. This rigorously justifies that the dynamics of the current and voltage controllers are systematically eliminated in the fifth-order model. Substituting the QSS solution for z into (17), we obtain the reduced fifth-order model of a single droop-controlled inverter:

$$\frac{d}{dt}\begin{bmatrix}\delta\\ S\\ i_\mathrm{o}\end{bmatrix}=\begin{bmatrix}\omega_\mathrm{nom}-m_\mathrm{P}\frac{S+S^*}{2}-\omega_\mathrm{com}\\ -\omega_\mathrm{c}S+\omega_\mathrm{c}v_\mathrm{o}^\mathrm{ref}i_\mathrm{o}^*\\ -\left(\frac{R_\mathrm{c}}{L_\mathrm{c}}+\mathrm{j}\omega\right)i_\mathrm{o}+\frac{v_\mathrm{o}^\mathrm{ref}-u}{L_\mathrm{c}}\end{bmatrix}, \tag{27}$$

where only the power angle, apparent power, and output current dynamics are retained as dynamic states, and the dynamics of the voltage controller and current controller are systematically eliminated (notice they can be recovered using the algebraic relations in (26)).

Adopting the same procedure, we can reduce the fifth-order model to a third-order model by neglecting the dynamics of the inverter output-filter current. To this end, $x=[\delta,\ S]^\mathrm{T}$, $z=i_\mathrm{o}$, and the small perturbation parameter, $\varepsilon_3=\frac{L_\mathrm{c}}{R_\mathrm{c}}$. Finally, the third-order model can be further reduced to a single order model by eliminating the dynamics of the power controller. To this end, $x=\delta$, $z=S$, and the small perturbation parameter, $\varepsilon_4=\frac{1}{\omega_\mathrm{c}}$. The vector fields, $f(\cdot)$, $g(\cdot)$, the QSS solution of z, and the reduced order dynamical model, $\widetilde{f}(\cdot)$, for the fifth-, third-, and first-order models are listed in Table I.

Conceivably, the different reduced-order models are useful in different contexts. For instance, the original full-order model is useful for the design of the current and voltage controllers. Similarly, the fifth-order model can be utilized to analyze the performance of (or design) the output inductive filter. The third-order model is relevant in the design and verification of secondary- and tertiary-level controllers (see, e.g., [5], [38], [39]). Finally, the first-order model is applicable in long-term performance evaluation, and dynamic reliability assessment [27], [45].

IV. Numerical Case Studies

In Section III, we outlined the reduced-order models of droop-controlled inverters in islanded microgrids. To test the spatio-temporal reduced order models, a software package with a user-selectable model order has been developed in MATLAB. The simulations are performed on a personal computer with an Intel® Core™i7-2600 CPU @ 3.4GHz and 24.0 GB installed RAM. The purpose of the case studies is two fold. First, the accuracy and computational burden of simulating the reduced-order models is evaluated on a modified IEEE 37-bus system; the results are summarized in Section IV-A. Furthermore, based on Kron reduction, a systematic procedure for selecting droop coefficients is presented to minimize power losses and voltage deviations in the microgrid electrical network; simulation results to validate this method are presented in Section IV-B.

The standard IEEE 37-bus system was modified by adding seven inverters at certain buses as shown in Fig. 3. The test system is studied at the nominal voltage of $v_\mathrm{nom}=220\sqrt{3}\,\mathrm{V}$ and a nominal frequency $\omega_\mathrm{nom}=2\pi50\,\mathrm{rad\,s^{-1}}$. The switching frequency of the inverters is set to be $f_\mathrm{s}=8\,\mathrm{kHz}$. Loads are modeled as constant impedances, and seven inverters are added at buses 15, 18, 22, 24, 29, 33 and 34, as shown in Fig. 3. The inverter control parameters are adopted from [2] and listed in Table IV; while the network and load parameters are collected in Tables V and VI in Appendix A.

A. Original Model Compared to Reduced Models

To test the dynamic behavior of the reduced-order models, the load connected to bus 1 is stepped up (from $6.68\,\Omega$ to $4.58\,\Omega$) at $t = 0.1$s and then stepped down (from $4.58\,\Omega$ to $6.58\,\Omega$) at $t = 1.1$s. The time-domain simulation results for different reduced model orders are compared. Since the load is changed at bus 1, results from four electrically close inverters connected to buses 15, 18, 22, and 34 are focused on (see Fig. 3). The simulation results of the terminal voltage angle, active power, and reactive power of the four inverters are shown in Fig. 4 for the different model orders.

From the plots, we can conclude that the dynamical behaviors of the fifth-order model match very well with the original model. The third- and single-order model have a small steady-state error in the terminal voltage angle and active power. This is primarily caused by neglecting the inductance L_c in the third- and single-order models. Furthermore, the computational efficiency of the reduced-order models is also evaluated. The total computation time from startup to the load steps (i.e., for the total 2s simulation time) for the original ninth-, fifth-, and third-order models are $2.377\,$s, $1.753\,$s, and $0.788\,$s, respectively. The simulation time for the third-order model is less than one third of that required for the original model. This verifies that the spatio-temporal reduced-order models can significantly reduce computational burden. Two variants of the single-order model are tested. In one, the nonlinear algebraic equations (see Table I) are retained, while in the other, these are discarded. If the nonlinear algebraic equations are discarded, this amounts to assuming that the terminal voltages are fixed (as is done, e.g., in the derivation of the classical model for synchronous generators in bulk power systems). The simulation times for these two variants are $0.824\,$s, and $0.486\,$s, respectively. While the simulation time can be reduced to a sixth of the original model by assuming the voltages are fixed, this variant of the single-order model is patently less accurate.

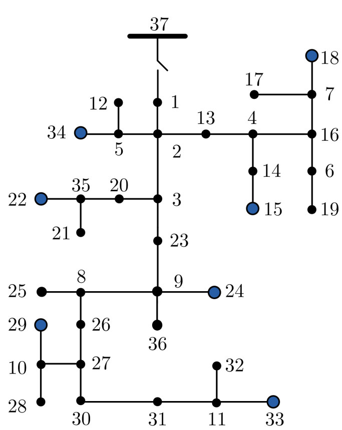

Figure 3: One-line diagram of modified IEEE 37-bus test system (inverters are represented by blue dots)

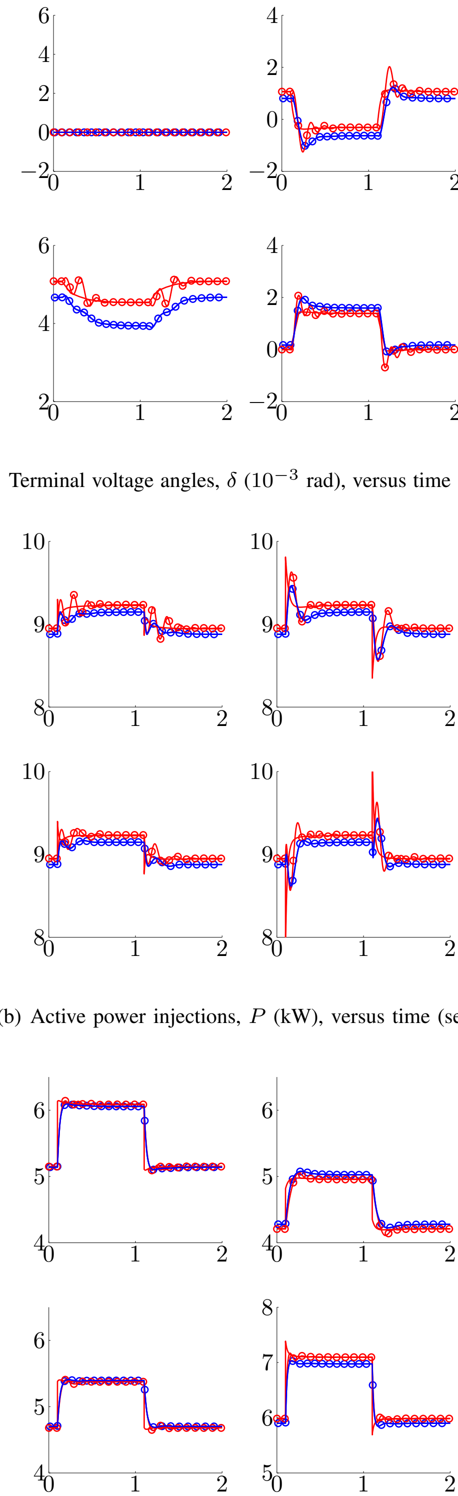

(a) Terminal voltage angles, δ (10^{-3} rad), versus time (sec.)

(b) Active power injections, P (kW), versus time (sec.)

(c) Reactive power injections, Q (kVAR), versus time (sec.)

Figure 4: Comparing the original and the reduced models for the response of four inverters in the modified IEEE 37-bus system to load steps. Clockwise from the upper left corner are waveforms for inverters connected to buses 15, 18, 34, and 22. Full order model is in solid blue, fifth-order model is in dotted blue, third-order model is in dotted red, and single-order model is in solid red.

B. Systematic Design of Droop Coefficients

Typically, droop coefficients for inverters in islanded inverters are selected to be equal, see, e.g., [2], [5]. From a system-level perspective, this implies that loads are meant to be shared equally by the inverters (assuming they have the same rating). This strategy is perhaps justifiable in lossless networks. However, in general, microgrids are resistive-dominant networks, and network power losses become an important design consideration. A useful strategy then, is to ensure that inverters meet the loads that are electrically closest to them. This would minimize power flows between inverters—effectively reducing losses as well as voltage deviations in the network. To this end, we propose a systematic strategy to select the droop coefficients inspired by the insights offered by Kron reduction which clearly illustrates the equivalent loads that the inverters have to support, as well as isolates the mutual inverter interactions.

Assume the nominal frequency (voltage) of all inverters are the same and denoted as ω_{nom} (v_{nom}). With regard to the Kron-reduced network, the equivalent load impedance of a given inverter is denoted by Z_{eq} (recall from (16) that this can be recovered from the appropriate diagonal entry of Y_{eq}). Therefore, the equivalent real and reactive power loads for the inverter are approximately given by

$$S_{\mathrm{eq}} = P_{\mathrm{eq}} + \mathrm{j}Q_{\mathrm{eq}} = \frac{v_{\mathrm{nom}}^2}{(Z_{\mathrm{eq}})^*}. \tag{28}$$

If the droop coefficients m_{P} and n_{Q} are picked to be:

$$m_{\mathrm{P}} = \frac{\omega_{\mathrm{nom}} - \omega_{\mathrm{com}}}{P_{\mathrm{eq}}}, \quad n_{\mathrm{Q}} = \frac{v_{\mathrm{nom}} - v_{\mathrm{o}}^{\mathrm{ref}}}{Q_{\mathrm{eq}}}, \tag{29}$$

Then it is straightforward to show from (1)-(4) that the steady state active- and reactive-power delivered by the inverter is given by that demanded by the equivalent loads P_{eq} and Q_{eq}. However, since we do not a priori know the values of ω_{com} and $v_{\mathrm{o}}^{\mathrm{ref}}$, a heuristic design choice is to set for each inverter:

$$m_{\mathrm{P}} = \frac{\Delta\omega \cdot \omega_{\mathrm{nom}}}{P_{\mathrm{eq}}}, \quad n_{\mathrm{Q}} = \frac{\Delta v_{\mathrm{nom}} \cdot v_{\mathrm{nom}}}{Q_{\mathrm{eq}}}, \tag{30}$$

where $\Delta\omega$ and Δv_{nom} are the tolerable frequency and voltage deviations.

For the modified IEEE 37-bus system in Fig. 3, the equivalent loads of the inverters computed using (28), and the droop coefficients designed using (30) are listed in Table II. To validate the strategy highlighted above, we consider two scenarios. In the first, we use uniform droop coefficients for all inverters ($m_{\mathrm{P}} = 5.9 \times 10^{-5}$ and $n_{\mathrm{Q}} = 3.3 \times 10^{-3}$, designed based on equally rated inverters $P_{\max} = 9.582\,\mathrm{kW}$, $Q_{\max} = 4.677\,\mathrm{kVAR}$). In the second scenario, we pick the droop coefficients in Table II. A load step at bus 12 is effected by changing the load from $49.93\,\Omega$ to $29.93\,\Omega$. The evolution of the terminal voltage angle, active power, and reactive power of the inverters for the two scenarios are shown in Fig. 5.

We see that when the droop coefficients are selected uniformly, all the inverters respond uniformly to the load step (i.e., they contribute the same active power to support the load change) (see Fig. 5(a)). With the droop coefficients selected based on (29), the inverters contribute different active powers (reactive powers) to support the frequency (voltage), since they tend to focus on balancing the equivalent local loads. The power losses and maximum voltage deviations in steady state (both before and after the load step) are shown in Table III. Compared to the case where all inverters have uniform droop coefficients, the network power losses and maximum voltage deviation are significantly lowered with the suggested design strategy.

The suggested approach requires knowledge of the Kron-reduced network. To this end, the effective impedances (and therefore, the Kron reduced circuit) can be recovered utilizing off-line measurements made at the inverter terminals [26], [46], [47], or by on-line topology identification approaches when time-synchronized measurements are available [48], [49].

Table II: Equivalent local loads and designed droop coefficients

Bus	P_{eq} (kW)	Q_{eq} (kVAR)	$m_{\mathrm{P}}(\times 10^{-5})$	$n_{\mathrm{Q}}(\times 10^{-3})$
15	10.415	5.041	3.770	3.0
18	7.294	3.593	5.383	4.2
22	9.987	4.943	3.932	3.1
24	8.946	4.218	4.490	3.6
29	5.338	2.600	7.357	5.9
33	9.681	4.726	4.058	3.2
34	15.598	7.611	2.517	2.0

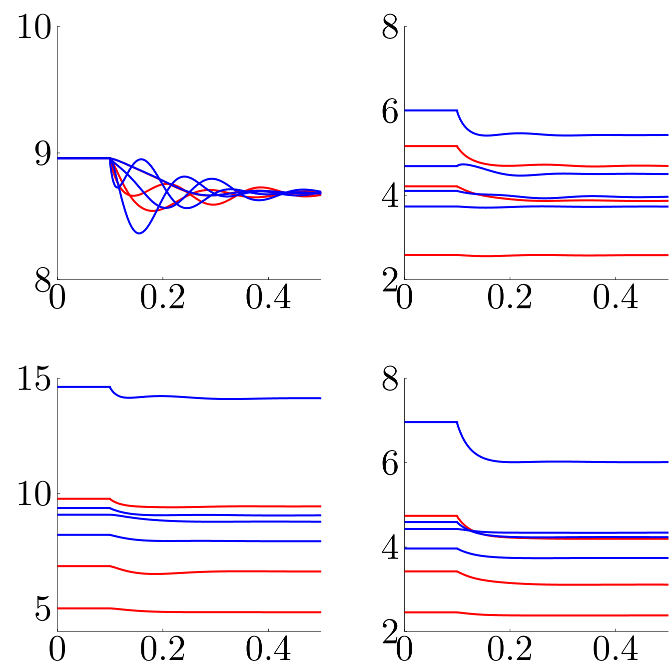

Figure 5: Step responses of the seven inverters (Clockwise from up-left corner: plots of P (kW, Scenario 1); Q (kVar, Scenario 1); Q (kVar, Scenario 2), P (kW, Scenario 2). All waveforms are plotted against time (sec). Notice that the active power output response of the inverters with the suggested design strategy is different for different inverters based on their local equivalent load.

Table III: Comparison of power losses and voltage deviations.

	Scenario 1		Scenario 2	
	Before	After	Before	After
Power losses (W)	153.98	170.04	0.124	1.336
Max voltage deviation (V)	23.92	25.26	0.840	0.884

V. Concluding Remarks and Directions for Future Work

In this paper, model reduction methods are proposed for systematically reducing large-signal dynamic models of droop-controlled inverters in islanded microgrids. The accuracy of the reduced-order models is verified with numerical simulations to accurately describe the original dynamics of the system. Also, we note that the reduced models offer significantly lower computational burden as compared to the original nonlinear models. Indeed, with the inevitable large-scale proliferation of power electronics circuits in microgrids, the computational benefits of model-reduction methods will be appreciated in all aspects of microgrids modeling, analysis, and control. In addition, spatial model reduction based on Kron reduction is employed to isolate the mutual inverter interactions and clearly illustrate the equivalent loads that the inverters have to support in the microgrid. Based on the Kron-reduced network model, a systematic approach to select the droop coefficients is proposed to minimize the power losses and voltage deviations. The models proposed in this paper are expected to aid future efforts in modeling, analysis, and control of microgrids. In particular, we will leverage the reduced-order models for the design of sparse control architectures for secondary-level control. As part of future work, we will also integrate constant-power loads into the analytical framework and consider grid-connected operation (as well as transitions between grid-connected and islanded modes). Furthermore, note that in the present setup, to leverage Kron reduction we assume quasi-stationary operation of the electrical network. Future efforts could involve leveraging the insights in, e.g., [50] to jointly consider transient behaviors while accomplishing the spatial model reduction objectives afforded by Kron reduction. Finally, an important direction is to establish robustness of the strategy suggested to design droop coefficients by leveraging insights from Kron reduction and algebraic power flow relationships. Validation with simulations of the nonlinear models and experimental prototypes will also be undertaken.

References

[1] M. Chandorkar, D. Divan, and R. Adapa, "Control of parallel connected inverters in standalone ac supply systems," *IEEE Trans. Ind. Appl.*, vol. 29, pp. 136–143, Jan. 1993.

[2] N. Pogaku, M. Prodanovic, and T. Green, "Modeling, analysis and testing of autonomous operation of an inverter-based microgrid," *Power Electronics, IEEE Transactions on*, vol. 22, pp. 613 –625, march 2007.

[3] G. S. Ladde and D. D. Siljak, "Multiparameter singular perturbations of linear systems with multiple time scales," *Automatica*, vol. 19, no. 4, pp. 385–394, 1983.

[4] S. Bae and A. Kwasinski, "Dynamic modeling and operation strategy for a microgrid with wind and photovoltaic resources," *Smart Grid, IEEE Transactions on*, vol. 3, pp. 1867 –1876, dec. 2012.

[5] A. Bidram and A. Davoudi, "Hierarchical structure of microgrids control system," *Smart Grid, IEEE Transactions on*, vol. 3, no. 4, pp. 1963–1976, 2012.

[6] A. Bidram, A. Davoudi, F. Lewis, and J. Guerrero, "Distributed cooperative secondary control of microgrids using feedback linearization," *Power Systems, IEEE Transactions on*, vol. 28, no. 3, pp. 3462–3470, 2013.

[7] D. Chaniotis and M. A. Pai, "Model reduction in power systems using krylov subspace methods," *Power Systems, IEEE Transactions on*, vol. 20, no. 2, pp. 888–894, 2005.

[8] F. Freitas, J. Rommes, and N. Martins, "Gramian-based reduction method applied to large sparse power system descriptor models," *Power Systems, IEEE Transactions on*, vol. 23, no. 3, pp. 1258–1270, 2008.

[9] J. Chow, R. Galarza, P. Accari, and W. Price, "Inertial and slow coherency aggregation algorithms for power system dynamic model reduction," *Power Systems, IEEE Transactions on*, vol. 10, no. 2, pp. 680–685, 1995.

[10] E. Abed and R. Silva-Madriz, "Stability of systems with multiple very small and very large parasitics," *Circuits and Systems, IEEE Transactions on*, vol. 34, no. 9, pp. 1107–1110, 1987.

[11] H. Khalil, *Nonlinear Systems*. Upper Saddle River, NJ: Prentice Hall, 2002.

[12] H. Khalil, "Stability analysis of nonlinear multiparameter singularly perturbed systems," *Automatic Control, IEEE Transactions on*, vol. 32, no. 3, pp. 260–263, 1987.

[13] G. Xu and V. Vittal, "Slow coherency based cutset determination algorithm for large power systems," *Power Systems, IEEE Transactions on*, vol. 25, no. 2, pp. 877–884, 2010.

[14] G. Xu, V. Vittal, A. Meklin, and J. Thalman, "Controlled islanding demonstrations on the wecc system," *Power Systems, IEEE Transactions on*, vol. 26, no. 1, pp. 334–343, 2011.

[15] P. V. Kokotovic, R. Malley, and P. Sannuti, "Singular perturbations and order reduction in control theory an overview," *Automatica*, vol. 12, pp. 123–132, 1976.

[16] H. K. Khalil, "Asymptotic stability of nonlinear multiparameter singularly perturbed systems," *Automatica*, vol. 17, no. 1, pp. 797–804, 1978.

[17] X. Xu, R. M. Mathur, J. Jiang, G. Rogers, and P. Kundur, "Modeling of generators and their controls in power system simulations using singular perturbations," *Power Systems, IEEE Transactions on*, vol. 13, no. 1, pp. 109–114, 1998.

[18] J. H. Chow, "Asymptotic stability of a class of nonlinear singularity perturbed systems," *J. Franklin Inst.*, vol. 305, pp. 123–132, 1978.

[19] V. Mariani, F. Vasca, and J. M. Guerrero, "Analysis of droop controlled parallel inverters in islanded microgrids," in *IEEE International Energy Conference (ENERGYCON)*, pp. 1304–1309, May 2014.

[20] J. Kimball and P. Krein, "Singular Perturbation Theory for DC-DC Converters and Application to PFC Converters," *IEEE Transactions on Power Electronics,*, vol. 23, pp. 2970–2981, Nov. 2008.

[21] A. Davoudi, J. Jatskevich, P. L. Chapman, and A. Bidram, "Multi-resolution modeling of power electronics circuits using model-order reduction techniques," *IEEE Transactions on Circuits and Systems I: Regular Papers*, vol. 60, pp. 810–823, March 2013.

[22] J. D. Owens and P. L. Chapman, "Automatic generation of accurate low-order models for magnetic devices," *IEEE Transactions on Power Electronics*, vol. 20, pp. 732–742, July 2005.

[23] A. Davoudi, P. L. Chapman, J. Jatskevich, and H. Behjati, "Reduced-order dynamic modeling of multiple-winding power electronic magnetic components," *IEEE Transactions on Power Electronics*, vol. 27, pp. 2220–2226, May 2012.

[24] G. Kron, "A method to solve very large physical systems in easy stages," *Circuit Theory, Transactions of the IRE Professional Group on*, vol. PGCT-2, pp. 71–90, 1953.

[25] R. Ciric, A. Padilha Feltrin, and L. Ochoa, "Power flow in four-wire distribution networks-general approach," *Power Systems, IEEE Transactions on*, vol. 18, no. 4, pp. 1283–1290, 2003.

[26] F. Dörfler and F. Bullo, "Kron reduction of graphs with applications to electrical networks," *Circuits and Systems I: Regular Papers, IEEE Transactions on*, vol. 60, no. 1, pp. 150–163, 2013.

[27] I.-Y. Chung, W. Liu, D. Cartes, J. Collins, E.G., and S.-I. Moon, "Control methods of inverter-interfaced distributed generators in a microgrid system," *Industry Applications, IEEE Transactions on*, vol. 46, no. 3, pp. 1078–1088, 2010.

[28] M. Hassan and M. Abido, "Optimal design of microgrids in autonomous and grid-connected modes using particle swarm optimization," *Power Electronics, IEEE Transactions on*, vol. 26, no. 3, pp. 755–769, 2011.

[29] J. Kim, J. Guerrero, P. Rodriguez, R. Teodorescu, and K. Nam, "Mode adaptive droop control with virtual output impedances for an inverter-based flexible ac microgrid," *Power Electronics, IEEE Transactions on*, vol. 26, no. 3, pp. 689–701, 2011.

[30] S. Dasgupta, S. Sahoo, and S. Panda, "Single-phase inverter control techniques for interfacing renewable energy sources with microgrid; part i: Parallel-connected inverter topology with active and reactive power flow control along with grid current shaping," *Power Electronics, IEEE Transactions on*, vol. 26, no. 3, pp. 717–731, 2011.

[31] M. Zhu, H. Li, and X. Li, "Improved state-space model and analysis of islanding inverter-based microgrid," in *Industrial Electronics (ISIE), 2013 IEEE International Symposium on*, pp. 1–5, 2013.

[32] A. Radwan and Y.-R. Mohamed, "Analysis and active-impedance-based stabilization of voltage-source-rectifier loads in grid-connected and isolated microgrid applications," *Sustainable Energy, IEEE Transactions on*, vol. 4, no. 3, pp. 563–576, 2013.

[33] J. Vasquez, J. Guerrero, M. Savaghebi, J. Eloy-Garcia, and R. Teodorescu, "Modeling, analysis, and design of stationary-reference-frame droop-controlled parallel three-phase voltage source inverters," *Industrial Electronics, IEEE Transactions on*, vol. 60, no. 4, pp. 1271–1280, 2013.

[34] J. W. Simpson-Porco, F. Dörfler, and F. Bullo, "Synchronization and power sharing for droop-controlled inverters in islanded microgrids," *Automatica*, vol. 49, no. 9, pp. 2603–2611, 2013.

[35] X. Lu, K. Sun, J. Guerrero, J. Vasquez, and L. Huang, "State-of-Charge Balance Using Adaptive Droop Control for Distributed Energy Storage Systems in DC Microgrid Applications," *IEEE Transactions on Industrial Electronics*, vol. 61, pp. 2804–2815, June 2014.

[36] F. Dörfler, J. W. Simpson-Porco, and F. Bullo, "Breaking the hierarchy: Distributed control & economic optimality in microgrids," *IEEE Transactions on Control of Network Systems*, January 2014. Submitted.

[37] Q.-C. Zhong, "Robust droop controller for accurate proportional load sharing among inverters operated in parallel," *Industrial Electronics, IEEE Transactions on*, vol. 60, no. 4, pp. 1281–1290, 2013.

[38] J. Guerrero, J. Vasquez, J. Matas, L. de Vicuna, and M. Castilla, "Hierarchical control of droop-controlled ac and dc microgrids - a general approach toward standardization," *Industrial Electronics, IEEE Transactions on*, vol. 58, no. 1, pp. 158–172, 2011.

[39] Y. Mohamed and A. Radwan, "Hierarchical control system for robust microgrid operation and seamless mode transfer in active distribution systems," *Smart Grid, IEEE Transactions on*, vol. 2, pp. 352 –362, june 2011.

[40] R. A. Horn and C. R. Johnson, *Matrix analysis*. Cambridge university press, 2012.

[41] S. V. Dhople, B. B. Johnson, F. Dörfler, and A. O. Hamadeh, "Synchronization of Nonlinear Circuits in Dynamic Electrical Networks with General Topologies," *IEEE Transactions on Circuits and Systems I: Regular Papers*, October 2013. To appear. Available at http://arxiv.org/abs/1310.4550.

[42] M. A. Pai, *Power System Stability: Analysis by the Direct Method of Lyapunov*. North-Holland systems and control series, North-Holland Publishing Company, 1981.

[43] H. Khalil, "Stability analysis of nonlinear multiparameter singularly perturbed systems," in *American Control Conference, 1987*, pp. 1219–1223, 1987.

[44] D. Peponides, P. V. Kokotovic, and J. H. Chow, "Singular perturbations and time scales in nonlinear models of power system," *Circuits and Systems, IEEE Transactions on*, vol. 29, no. 11, pp. 758–767, 1982.

[45] S. V. Dhople, Y. C. Chen, L. DeVille, and A. D. Domínguez-García, "Analysis of power system dynamics subject to stochastic power injections," *IEEE Transactions on Circuits and Systems I: Regular Papers*, vol. 60, pp. 3341–3353, December 2013.

[46] A. M. Ehrlich, "Parallel and series addition of networks," 1996. Tech. report, REU Mathematics Project, University of Washington, [Online] Available at: `http://math.washington.edu/ reu`.

[47] N. Saksena, "The Dirichlet problem for infinite networks," 2002. Tech. report, REU Mathematics Project, University of Washington, [Online] Available at: `http://math.washington.edu/ reu`.

[48] S. Nabavi and A. Chakrabortty, "Topology Identification in Dynamic Equivalent Models of Power Systems," *IEEE Transactions on Power Systems*, 2013, in review.

[49] S. Nabavi and A. Chakrabortty, "Topology identification for dynamic equivalent models of large power system networks," in *American Control Conference*, pp. 1138–1143, June 2013.

[50] S. Caliskan and P. Tabuada, "Kron reduction of power networks with lossy and dynamic transmission lines," in *IEEE 51st Annual Conference on Decision and Control*, pp. 5554–5559, Dec. 2012.

Appendix A
Simulation Parameters For Inverters and Network

Table IV: Inverter controller parameters [2]

Parameter	Value	Parameter	Value
ω_{c}	31.41	F	0.75
K_{p}^{ϕ}	0.05	K_{i}^{ϕ}	390
K_{p}^{γ}	10.5	K_{i}^{γ}	16×10^3
L_{f}	1.35 mH	R_{f}	0.1 Ω
L_{c}	0.35 mH	R_{c}	0.03 Ω

Table V: Branch parameters

From	To	R	L	From	To	R	L
1	2	0.167	2.31×10^{-4}	10	29	0.223	3.08×10^{-4}
2	5	0.070	9.64×10^{-5}	11	33	0.070	9.64×10^{-5}
2	13	0.063	8.67×10^{-5}	11	32	0.035	4.82×10^{-5}
2	3	0.230	3.18×10^{-4}	13	4	0.091	1.25×10^{-4}
3	20	0.042	5.78×10^{-5}	14	15	0.091	1.25×10^{-4}
3	23	0.105	1.45×10^{-4}	16	7	0.160	2.22×10^{-4}
4	14	0.014	1.93×10^{-5}	16	6	0.105	1.45×10^{-4}
4	16	0.139	1.93×10^{-4}	20	35	0.049	6.75×10^{-5}
5	34	0.056	7.71×10^{-5}	23	9	0.035	4.82×10^{-5}
5	12	0.042	5.78×10^{-5}	26	27	0.098	1.35×10^{-4}
6	19	0.049	6.75×10^{-5}	27	30	0.112	1.54×10^{-4}
7	18	0.132	1.83×10^{-4}	27	10	0.091	1.25×10^{-4}
7	17	0.021	2.89×10^{-5}	30	31	0.070	9.64×10^{-5}
8	26	0.056	7.71×10^{-5}	31	11	0.070	9.64×10^{-5}
8	25	0.056	7.71×10^{-5}	35	21	0.035	4.82×10^{-5}
9	24	0.105	1.45×10^{-4}	35	22	0.049	6.75×10^{-5}
9	8	0.056	7.71×10^{-5}	36	9	0.230	3.18×10^{-4}
10	28	0.035	4.82×10^{-5}				

Table VI: Load parameters

Bus	R	L	Bus	R	L
1	6.58	0.0105	24	49.93	0.0748
12	49.93	0.0748	25	98.74	0.1572
13	49.93	0.0748	26	49.93	0.0748
14	111.41	0.1681	27	98.74	0.1572
15	49.93	0.0748	28	49.93	0.0748
16	49.93	0.0748	29	98.74	0.1572
17	25.82	0.0409	30	29.62	0.0472
18	98.74	0.1572	31	33.12	0.0519
19	98.74	0.1572	32	49.93	0.0748
20	98.74	0.1572	33	98.74	0.1572
21	32.91	0.0524	34	45.54	0.0686
22	98.74	0.1572	35	98.74	0.1572
23	49.93	0.0748			

Ling Luo received the B.S. and M.S. degrees in Electrical Engineering, in 2004 and 2007, respectively, from Huazhong University of Science and Technology, Wuhan, China. She received an M.S. degree in Electrical Engineering in 2014 from the University of Minnesota, Minneapolis, MN. Her research interests include power system stability and control, distributed generation, and microgrid modeling.

Sairaj V. Dhople (S'09, M'13) received the B.S., M.S., and Ph.D. degrees in electrical engineering, in 2007, 2009, and 2012, respectively, from the University of Illinois, Urbana-Champaign. He is currently an Assistant Professor in the Department of Electrical and Computer Engineering at the University of Minnesota (Minneapolis), where he is affiliated with the Power and Energy Systems research group. His research interests include modeling, analysis, and control of power electronics and power systems with a focus on renewable integration.